The Fas–FADD death domain complex structure reveals the basis of DISC assembly and disease mutations

Liwei Wang[1,8,9], Jin Kuk Yang[1,2,9], Venkataraman Kabaleeswaran[1,9], Amanda J Rice[3], Anthony C Cruz[4], Ah Young Park[5], Qian Yin[1], Ermelinda Damko[1], Se Bok Jang[1,6], Stefan Raunser[3,8], Carol V Robinson[5], Richard M Siegel[4], Thomas Walz[3,7] & Hao Wu[1]

The death-inducing signaling complex (DISC) formed by the death receptor Fas, the adaptor protein FADD and caspase-8 mediates the extrinsic apoptotic program. Mutations in Fas that disrupt the DISC cause autoimmune lymphoproliferative syndrome (ALPS). Here we show that the Fas–FADD death domain (DD) complex forms an asymmetric oligomeric structure composed of 5–7 Fas DD and 5 FADD DD, whose interfaces harbor ALPS-associated mutations. Structure-based mutations disrupt the Fas–FADD interaction *in vitro* and in living cells; the severity of a mutation correlates with the number of occurrences of a particular interaction in the structure. The highly oligomeric structure explains the requirement for hexameric or membrane-bound FasL in Fas signaling. It also predicts strong dominant negative effects from Fas mutations, which are confirmed by signaling assays. The structure optimally positions the FADD death effector domain (DED) to interact with the caspase-8 DED for caspase recruitment and higher-order aggregation.

Death domains share a common six–α-helical bundle structure[1,2] and are versatile modules of protein-protein interactions that mediate the assembly of numerous caspase-activating and NF-κB–activating complexes in apoptotic and inflammatory signaling including the DISC[3–6]. Our current understanding of the Fas DD–FADD DD interaction is both conflicting and confusing. The structures of Fas DD and FADD DD have long been elucidated by the NMR method, with the Fas DD structure determined under an acidic condition that disrupts the protein's capacity to oligomerize and to interact with FADD DD[7–9]. Extensive mutagenesis has been performed, but the disruptive mutations map to expanded surfaces with no well-defined patches[7,9–11]. The same is true for locations of disease-associated mutations in Fas DD[12–15].

Furthermore, in a structure of the complex that was crystallized in 0.95 M citric acid and 1.9 M ammonium sulfate at pH 4.0, these ALPS-associated disease-causing mutations in Fas DD are not localized at the interfaces with FADD DD[16]. Here we present a different structure of this complex that was crystallized in low salt and more neutral pH and that agrees well with electron microscopy, mass spectrometry and multi-angle light scattering studies in regard to the shape, size and stoichiometry of the complex in solution. The structure reveals the molecular basis of ALPS mutations, was further validated by structure-based mutagenesis both *in vitro* and in cells, and provides an elegant framework for optimal interaction with Fas ligand and for caspase recruitment and activation.

RESULTS

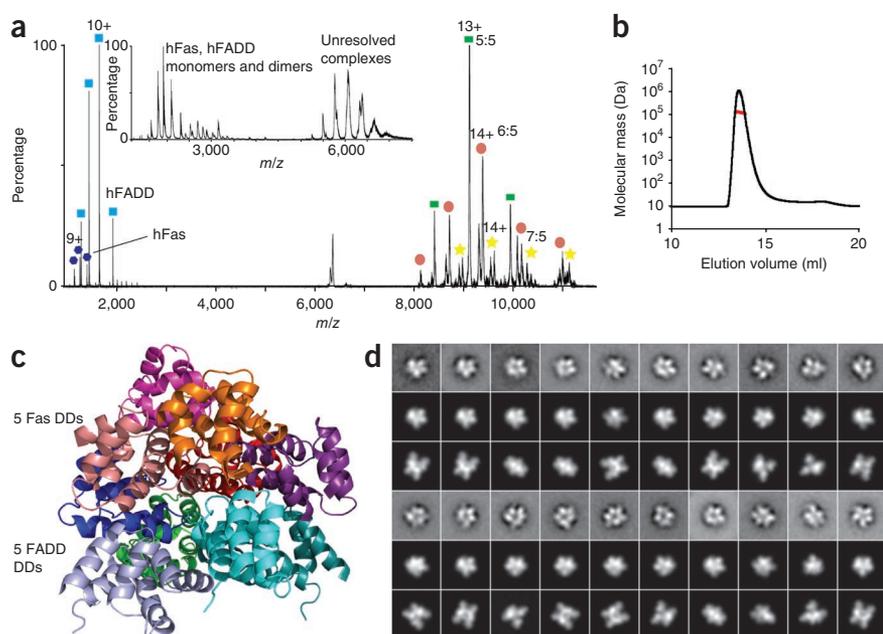### Similarity of the Fas–FADD complex to the PIDD–RAIDD complex

To resolve the conflicting data and to clarify the molecular basis of DD interactions in the DISC, we reconstituted the human Fas (hFas) DD–human FADD (hFADD) DD complex (**Supplementary Fig. 1a**) and the mouse Fas (mFas) DD–hFADD DD complex and used electron microscopy (EM) to visualize the structures of the complexes. EM of negatively stained Fas DD–FADD DD complexes revealed monodisperse and homogeneous particle populations (**Supplementary Fig. 1b**). Classification of 10,397 particles of the hFas–hFADD complex and 15,271 particles of the mFas–hFADD complex into 100 groups produced class averages that revealed molecules of similar size, about 10 nm in diameter, but with varying structural features (**Supplementary Fig. 1c,d**), indicative of different orientations of the complex on the carbon support film. The EM averages of the hFas–hFADD and the mFas–hFADD complexes are visually indistinguishable.

Unexpectedly, both the size and the appearance of Fas DD–FADD DD EM projections looked similar to the EM averages of the layered structure of the oligomeric PIDD DD–RAIDD DD complex[17] (**Supplementary Fig. 1e**). In this complex, a layer of five RAIDD molecules is sandwiched between a layer of five PIDD molecules on one side and two additional, loosely associated RAIDD molecules on the other side[17]. To provide more confidence in this assessment, we used nanoflow electrospray ionization and tandem mass spectrometry

[1]Department of Biochemistry, Weill Cornell Medical College, New York, New York, USA. [2]Department of Chemistry, Soongsil University, Seoul, Korea. [3]Department of Cell Biology, Harvard Medical School, Boston, Massachusetts, USA. [4]National Institute of Arthritis and Musculoskeletal and Skin Diseases, National Institutes of Health, Bethesda, Maryland, USA. [5]Department of Chemistry, University of Oxford, Oxford, UK. [6]Department of Molecular Biology, Pusan National University, Busan, Korea. [7]Howard Hughes Medical Institute, Harvard Medical School, Boston, Massachusetts, USA. [8]Present addresses: National Laboratory of Biomacromolecules, Institute of Biophysics, Chinese Academy of Sciences, Beijing, China (L.W.); Max Planck Institute of Molecular Physiology, Dortmund, Germany (S.R.). [9]These authors contributed equally to this work. Correspondence should be addressed to H.W. (haowu@med.cornell.edu).

Figure 1 Biochemical and structural characterization of the Fas DD–FADD DD complexes. (**a**) Tandem mass spectrum of the hFas–hFADD complex showing the dissociated monomers and the 'stripped' complexes at high gas phase collisional activation. (**b**) A representative multi-angle light scattering (MALS) measurement of the hFas–hFADD complex. More MALS data are summarized in **Supplementary Table 1**. (**c**) Crystal structure of the core 5:5 mFas–hFADD complex. The Fas molecules are shown in warm colors and the FADD DD molecules are shown in cool colors. (**d**) Class averages of the mFas–hFadd complex (first and fourth lines) with best-matching projections from the current mFas–hFADD crystal structure (second and fifth lines) and from a previously published structure of the Fas–FADD complex (third and sixth lines)[16].

to characterize the stoichiometry of the complex. The data showed that the hFas–hFADD complex consists predominantly of a 5:5 species with minor populations of 6:5 and 7:5 species, whereas the mFas–hFADD complex consists predominantly of 5:5 and 6:5 species with a minor population of the 7:5 complex (**Fig. 1a** and **Supplementary Fig. 2a,b**). We then determined the size of the complexes quantitatively using multi-angle light scattering (MALS). Among the multiple measurements on multiple samples, a range of molecular masses was obtained, which is consistent with a 5 Fas–5 FADD core complex and loosely bound additional subunits (**Fig. 1b** and **Supplementary Table 1**). Therefore, both the mass spectrometry and the MALS measurements support the similarity of the 5–7 Fas DD and 5 FADD DD complex to the PIDD–RAIDD complex[17]. Although this result was unexpected and suggested that the structure of the Fas DD–FADD DD complex differs from the reported symmetrical tetrameric structure of the complex at high salt and pH 4.0 (ref. 16), it would agree with the minimal stoichiometry of the extracellular interaction between Fas and its ligand FasL (see below).

Table 1 Data collection and refinement statistics

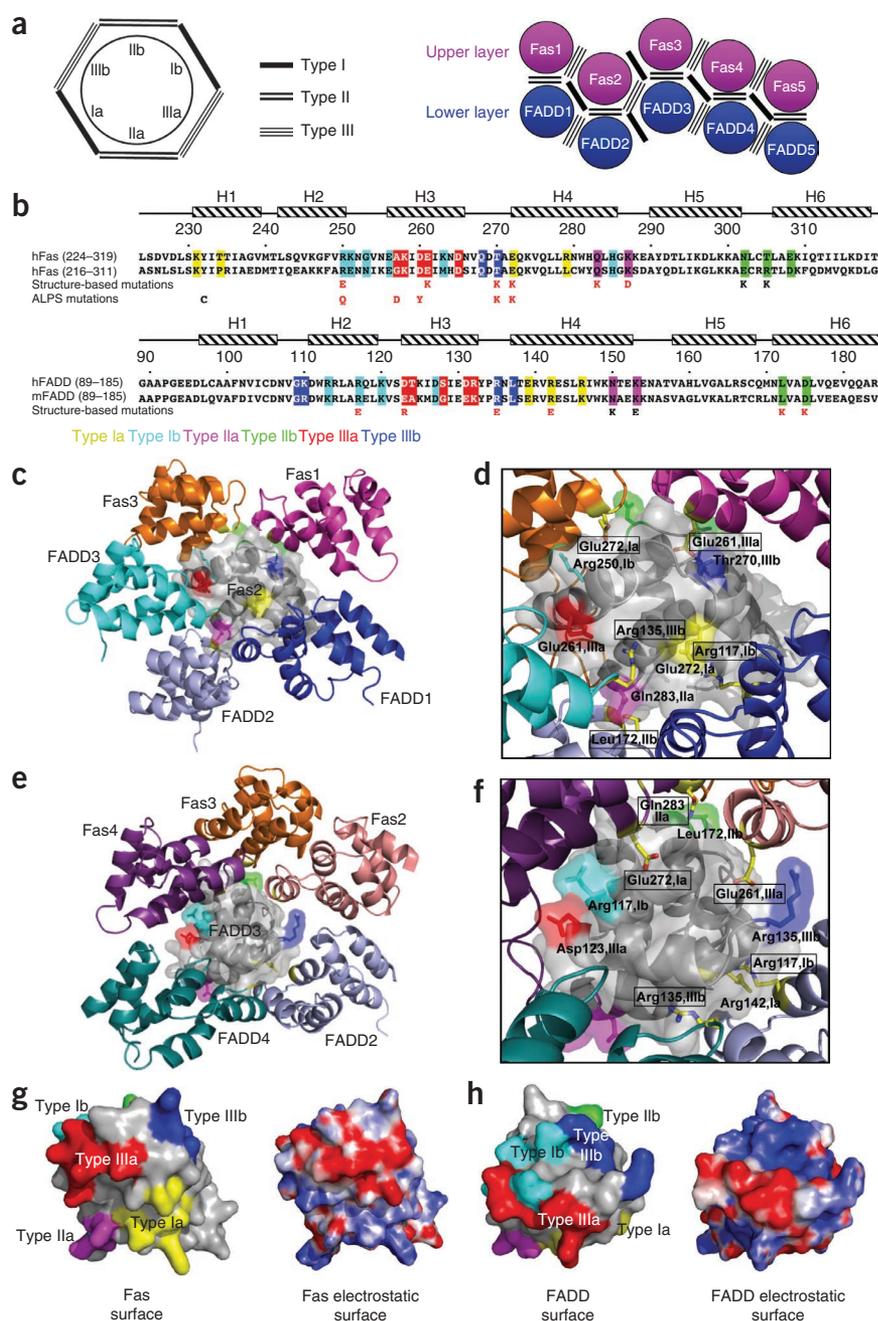|	mFas DD–hFADD DD complex
Data collection	
Space group	$C222_1$
Cell dimensions	
a, b, c (Å)	135.2, 144.5, 131.6
Resolution (Å)	50.0–6.8 (7.0)
R_{sym} (%)	7.0 (46.2)
$I / \sigma I$	28.0 (1.3)
Completeness (%)	93.0 (69.0)
Redundancy	4.9 (2.7)
Refinement	
Resolution (Å)	20–6.8
No. reflections	1,941
R_{work}/R_{free} (%)	35.4 / 34.9
No. atoms	
Protein	7,270
B-factors (Å^2)	451.6
R.m.s. deviations	
Bond lengths (Å)	0.014
Bond angles (°)	1.7

Values in parenthesis are for the highest-resolution shell.

Crystal structure of the core Fas–FADD DD complex

We were able to crystallize the mFas–hFADD complex and obtained its diffraction data at 6.8 Å resolution. We built a layer of five Fas DD and a layer of five FADD DD using the known structures of hFas and hFADD[7,16], respectively, based on the PIDD–RAIDD complex structure[17]. We then solved the structure of the complex by molecular replacement using the Fas DD layer and the FADD DD layer as models (**Table 1** and **Supplementary Table 2**). The availability of the individual Fas DD and FADD DD structures provided atomic details of the structure of the complex, which was shown to be a two-layered structure with an upper layer of five Fas DD molecules and a lower layer of five FADD DD molecules (**Fig. 1c**). This order of layers in the structure is consistent with the greater similarity between Fas and RAIDD and between FADD and PIDD (**Supplementary Fig. 3a**). The additional Fas molecules in the complex, which are equivalent to the additional RAIDD molecules in the PIDD–RAIDD complex, are not present in the mFas–hFADD crystal structure because of steric hindrance in crystal packing. The low resolution of the crystals may be reflective of the heterogeneity of the complex. Calculated re-projections of the crystal structure agree well with the experimental class averages (**Fig. 1d**). Differences in structural details are likely due to staining artifacts.

Structure-based mutations have semiquantitative effects

The Fas DD–FADD DD complexes are assembled via an elegant polymerization mechanism involving three types of asymmetric interactions at six unique interfaces that mediate Fas-FADD, Fas-Fas and FADD-FADD interactions (**Fig. 2a,b**). The type Ia surface composed of residues at the H1 and H4 helices interacts with the type Ib surface composed of residues at H2 and H3. The type IIa surface formed by residues at the H4 helix and the H4-H5 loop interacts with the type IIb surface at the H5-H6 loop and H6 helix. The type IIIa surface from residues at H3 interacts with the type IIIb surface formed by residues at the H1-H2 and the H3-H4 loops. The individual layers are assembled by five successive type I and type III interactions. The type II interactions only mediate the interactions between the layers. Type I and type III interfaces of both Fas DD and FADD DD should be critical for complex formation. For the type II interaction, only the type IIa surface of the Fas DD and the type IIb surface of the FADD DD should be important.

Figure 2 Interactions in the Fas DD–FADD DD complex. (**a**) Schematic planar diagram showing the construction of the complex. The locations of the three types of contacts are shown. (**b**) Sequence alignment of human and mouse Fas DD and FADD DD. Major interfacial residues are colored in yellow for type Ia, cyan for type Ib, magenta for type IIa, green for type IIb, red for type IIIa and blue for type IIIb. Single-letter codes below the sequences indicate mutations tested; red indicates mutations that are interaction defective and black those that are not. Locations of ALPS mutations are also shown. (**c**) Arrangement of molecules around Fas2, viewing into the schematic diagram in **a** from behind the page. (**d**) Zoom-in of **c** showing residues at the three types of interactions in Fas2 (labeled without a text box) and the surrounding molecules (labeled with a text box). Residues in Fas2 are colored as in **b** (residue name not labeled for type IIb). Side chains of residues in the surrounding molecules are shown as stick models colored by atom types. (**e**) Arrangement of molecules around FADD3, viewing into the schematic diagram in **a** from behind the page. (**f**) Zoom-in of **e** showing residues at the three types of interactions in FADD3 (labeled without a text box) and the surrounding molecules (labeled with a text box). Residues in FADD3 are colored as in **b** (residue name not labeled for type IIa). Side chains of residues in the surrounding molecules are shown as stick models colored by atom types. (**g**,**h**) Surface representations of Fas DD (**g**) and FADD DD (**h**) showing the locations of the three types of interactions (left) and the surface charge features (right).
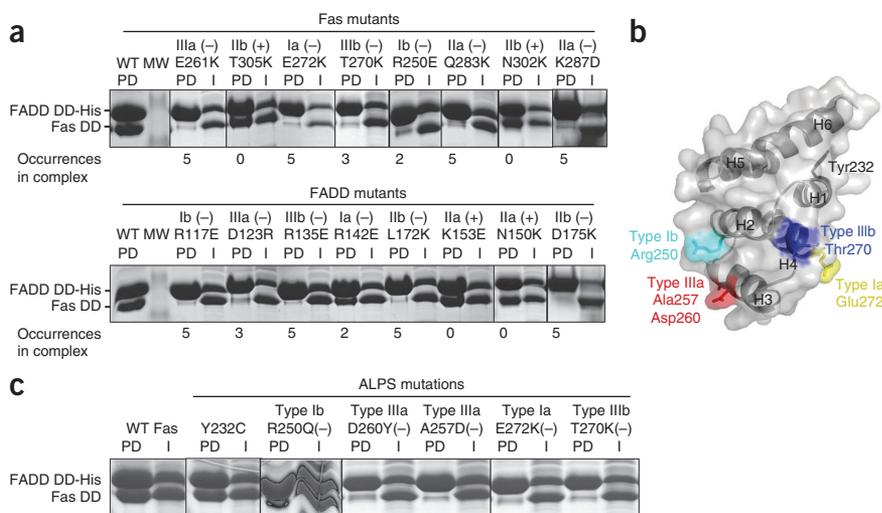
(type IIIb). More than half of the selected residues were either positively or negatively charged, consistent with the salt dependence of complex formation (**Supplementary Fig. 3b**) and suggesting that complex formation is to a considerable degree driven by electrostatic interactions (**Fig. 2g,h**).

Notably, all structure-based mutations at the predicted type I and type III interfaces caused severe disruption of the Fas DD-FADD DD interaction (**Figs. 2b** and **3a**). The type IIa mutations of the Fas DD disrupted the interaction but the type IIb mutations did not. Conversely, the type IIb mutations of the FADD DD disrupted the interaction, whereas the type IIa mutations did not. Consistent with their surface locations, none of the disruptive mutations affected the structural integrity of the DDs as shown by circular dichroism (CD) experiments (**Supplementary Fig. 3c**). The structure of the Fas–FADD complex was further validated by mutations on conserved surface residues that are not at the observed interface, which did not interfere with the Fas-FADD interaction (**Supplementary Fig. 3d**). Notably, there seems to be a semiquantitative correlation between the severity of the mutational phenotype and the extent of involvement of the interface in complex assembly. For example, the type Ib interface of Fas and the type Ia interface of FADD are only used twice in the complex in comparison with 3–5 times for the other types of interactions (**Fig. 2a**), explaining the somewhat weaker effects of the Fas R250E type Ib mutation and the FADD R142E type Ia mutation (**Fig. 3a**).

To rigorously confirm the structure, we took an unbiased approach to identify key residues at each of the interfaces in an equivalent hFas DD–hFADD DD complex (**Fig. 2b–f**). Residues that bury the most surface area were selected and mutated to charged residues that most likely would disrupt the interaction. One residue was chosen for each of the type I and type III interfaces in Fas DD and FADD DD. Two residues each were chosen for the type II interface to validate the relative layer positions of Fas DD and FADD DD. These mutations on Fas DD were E272K (type Ia), R250E (type Ib), Q283K (type IIa), K287D (type IIa), T305K (type IIb), N302K (type IIb), E261K (type IIIa) and T270K (type IIIb). The residue numbers are based on the human Fas precursor sequence, and 16 should be subtracted from each number for the mature sequence. The mutations on human FADD DD were R142E (type Ia), R117E (type Ib), K153E (type IIa), N150K (type IIa), L172K (type IIb), D175K (type IIb), D123R (type IIIa) and R135E

Figure 3 Structure-based mutagenesis and analysis of ALPS mutations. (**a**) Analysis of structure-based mutations of Fas DD and FADD DD in the *in vitro* His-tag pulldown assay. (–) indicates a defective interaction. PD, pulldown; I, input. (**b**) Mapping of ALPS-associated mutation residues onto the surface of Fas DD. (**c**) Pulldown of ALPS-associated Fas DD mutants by His-tagged FADD DD. (–) indicates a defective interaction. PD, pulldown; I, input.

Fas DD–FADD DD complex are dissimilar to the calculated projections of the tetrameric complex (**Fig. 1d** and **Supplementary Fig. 4d**). Because the reported Fas DD–FADD DD complex was crystallized in high salt and low pH[16], factors known to disrupt Fas DD interaction and function[7] (**Supplementary Fig. 3b**), it is likely that these conditions dramatically altered Fas conformation (**Supplementary Fig. 4e**), caused a remodeling of the complex and resulted in the non-physiological oligomer observed in the crystal[16].

In addition to Fas mutations that are associated with ALPS, there are extensive existing mutagenesis data on FADD DD[9,10]. Classifying the residues into three types of interactions allowed us to explain the observed effects of these FADD DD mutants on interactions with Fas DD (**Supplementary Table 4**). As expected, residues at these interfaces, especially those that are completely buried, caused disruption when mutated.

ALPS mutations map to interfaces in the Fas-FADD structure

Mutations in Fas are the most frequent causes of ALPS and, of these, about 70% are mutations in the intracellular DD[12–15]. To resolve whether our Fas DD–FADD DD complex could help clarify the structural mechanisms of ALPS, we analyzed naturally occurring Fas mutations associated with ALPS (http://research.nhgri.nih.gov/ALPS/fas_tnfrsf6_exon9_mut.shtml). Among the 20 single-site ALPS mutations in Fas DD, we selected those that do not involve glycine or proline and are exposed on the surface of the Fas DD (**Supplementary Table 3**). These mutations most likely do not influence the structural integrity of the Fas DD. If there were multiple mutations on the same residue, one mutation was chosen to simplify the analysis. Six mutations were selected: Y232C, R250Q, A257D, D260Y, T270K and E272K (**Fig. 3b**). Notably, three of the residues involved, Arg250, Thr270 and Glu272, are located at the centers of type Ib, IIIb and Ia interfaces, respectively. R250E (a mutation related to R250Q), T270K and E272K have already been tested in structure-based mutagenesis and shown to be defective in interacting with FADD DD. Residues Ala257 and Asp260 reside near the center of the type IIIa interface. In contrast, Tyr232 is located near the beginning of helix H1 (**Fig. 3b**).

Pulldown of wild-type and mutant Fas DD with histidine-tagged FADD DD showed that ALPS mutants R250Q, A257D and D260Y, as well as T270K and E272K, were severely defective in interaction with FADD DD (**Fig. 3c**). Lack of appreciable structural perturbation had been confirmed by earlier NMR studies for some of these mutations, including R250Q and A257D, as well as D260V, a mutation similar to D260Y[11]. The structural integrity of T270K and E272K was validated by CD measurements (**Supplementary Fig. 3c**). In contrast, the Y232C mutant interacted normally with FADD DD. In the family from which it was isolated, the Y232C Fas mutation inhibited apoptosis and caused ALPS only when coexpressed with an extracellular R137W mutation on the other allele, likely by reducing Fas surface expression[13].

The Fas DD–FADD DD structure we present here demonstrates that a majority of the Fas DD ALPS mutations exert their disease phenotypes through failure to form a complex with FADD DD. In contrast, none of the five ALPS mutations or the structurally identified disruptive mutations are located at the interface in the Fas DD–FADD DD crystal structure[16] (**Supplementary Fig. 4a–c**). Instead, they map onto the exposed surface of the symmetrical tetrameric complex. In addition, the experimental EM projections of the

Structure-based mutations disrupt Fas–FADD interaction *in vivo*

To determine the effects of Fas and FADD mutations on signaling complex formation in intact living cells, we performed fluorescence energy transfer (FRET) experiments on full-length Fas and the FADD DD (**Fig. 4a,b**). Full-length Fas and the FADD DD were fused to YFP and CFP, respectively, and coexpressed in 293T cells. FRET using GFP variants is a sensitive measure of protein-protein interactions at distances less than 10 nm[18]. Cells coexpressing full-length Fas and the FADD DD produced large FRET signals, indicating complex formation, whereas cells expressing a Fas mutant lacking the death domain (Fas ΔDD) had reduced FRET signals, indicating that FRET was dependent on DD-DD interactions. Notably, all mutant Fas and FADD constructs that were defective in the Fas DD-FADD DD interaction *in vitro* also had reduced FRET signals compared to the wild-type proteins, whereas the Fas and the FADD mutants that did not affect the Fas DD–FADD DD complex formation *in vitro* interacted normally with the complementary DD by FRET. The semiquantitative correlation between the number of occurrences of an interaction in the Fas DD–FADD DD complex and the mutational effect of that particular interaction appeared to be more prominent in living cells than *in vitro* (**Fig. 4a,b**).

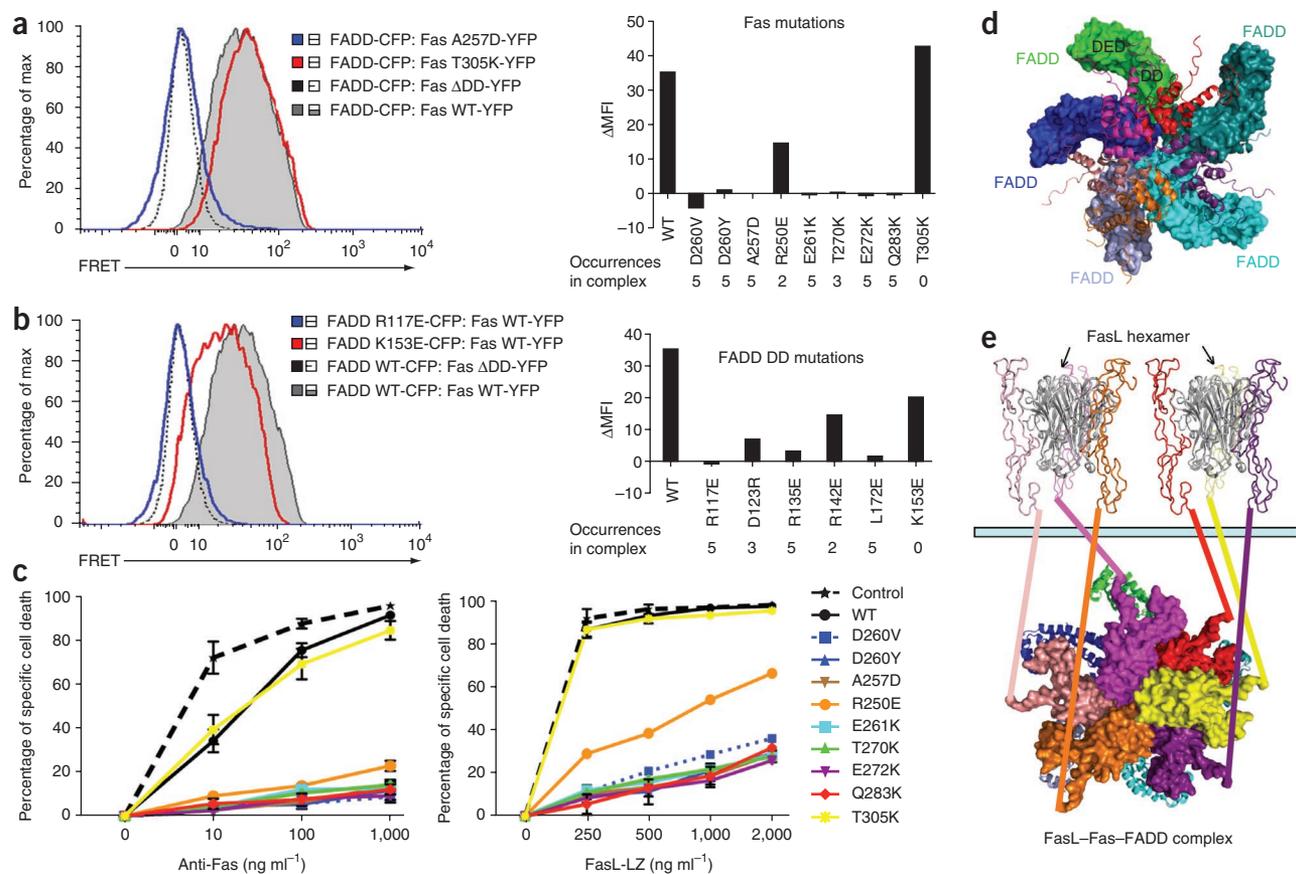## Dominant negative effects of structure-based and ALPS mutations

Almost all Fas DD mutations in ALPS are dominant and from a heterozygous background, which is consistent with the oligomeric nature and the high cooperativity of assembly of the Fas DD–FADD DD complex. ALPS-associated Fas mutations that cannot bind FADD interfere with Fas-induced apoptosis by dominantly disrupting the wild-type Fas from assembling the DISC[11,14,19]. Assuming the complete loss of function of a Fas mutant and a 1:1 mix of wild-type:mutant Fas in a heterozygous patient, the proportion of wild-type

Figure 4 Interactions in living cells and functional effects of Fas DD and FADD DD mutations. (**a**) Biexponential plot of the FRET signals for cells transfected with the indicated constructs (left) and the relative mean fluorescence intensities (ΔMFI) for WT and mutant Fas (right). The occurrences of the interactions in the complex are shown. (**b**) Same as **a**, but showing data for WT and mutant FADD DD. Results shown in **a** and **b** are representative of three independent experiments. (**c**) Effect of Fas DD mutants on Fas-induced cell death in transfected Jurkat E6.1 cells. Results are the average ± s.e.m. of specific cell death in three independent experiments. (**d**) Fas DD–full-length FADD complex model constructed by superimposing FADD DD with the structure of full-length FADD[20]. Fas DDs are shown in ribbon diagrams and FADD molecules in surface representations. Location of FADD DED for caspase-8 recruitment is shown for one of the FADD molecules. (**e**) Model for post-receptor DISC formation that uses FasL hexamerization. All structures are shown in ribbon diagrams except for the surface representations of the intracellular DDs of Fas. The two FasL trimers are shown in gray. The six Fas extracellular domains are shown in the same color as their intracellular death domains. A sixth Fas intracellular death domain (yellow) was added to the crystal structure (PMDB accession PM0076550). The extracellular and the intracellular domains are connected via straight lines of the same colors. Full-length FADD molecules are shown in ribbon diagrams. The light green bar represents the cellular membrane.

signaling complex would be <1/2[5], or ~3%, of total signaling complex, explaining the strong dominant negative phenotype of ALPS-associated Fas DD mutations.

To determine whether structure-based Fas mutants engineered to disrupt the Fas–FADD complex also act as dominant negatives, we transfected plasmids encoding these mutants fused to YFP into the Fas-sensitive T cell line Jurkat. As previously described[11], the ALPS-associated mutants A257D, D260Y and D260V almost completely abrogated apoptosis induced by either cross-linked anti-Fas antibody or FasL oligomerized through a leucine zipper tail (FasL-LZ) (**Fig. 4c**). As dominant negative mutants, the structure-based Fas mutants, Q283K, E272K, T270K and E261K, were as potent as the ALPS-associated Fas mutants. The R250E mutant was somewhat weaker but still showed more than 50% inhibition at most doses of anti-Fas or FasL-LZ (**Fig. 4c**). Residue Arg250 of Fas is at the type Ib interface that is less involved in complex formation than other types of interactions (**Fig. 2a**). The T305K IIb interface mutant that did not interfere with Fas–FADD complex formation had no inhibitory effect on Fas-induced apoptosis. Collectively, these data showed that the Fas DD–FADD DD structure correctly predicted the effects of both

structure-based and ALPS Fas mutants in interfering with wild-type Fas signaling complexes.

DISCUSSION

Model of the DISC and requirement for dimers of FasL trimers

Availability of the full-length FADD structure composed of both the DD and the death effector domain (DED)[20] allowed us to generate a model of the Fas DD in complex with full-length FADD (**Fig. 4d**). Notably, the DED domain of FADD does not have any steric clashes with the Fas DD–FADD DD structure and points toward the outside of the complex, poised for interaction with the DED domain of caspase-8.

Apoptosis is triggered by the membrane-bound form of FasL and cross-linked anti-Fas antibodies but not the proteolytically processed, trimeric soluble form of FasL[21–23]. When soluble trimeric FasL is dimerized into an engineered hexameric molecule, it is highly competent to signal apoptosis, suggesting that the minimal signaling-competent form of FasL is hexameric[24]. Notably, a dimer of FasL trimers would bring six Fas intracellular DDs into proximity, which is ideal in inducing the formation of the oligomeric complex composed of

5–7 Fas molecules (**Fig. 4e**). Because the DED domains of both FADD and caspase-8 are also capable of self-association[25,26], they can mediate further oligomerization of the DISC into microscopically visible clusters[27] to facilitate optimal caspase-8 clustering and activation. Cell death should have an intricately controlled threshold with sensitivity to ligand stimulation and protection from accidental firing. The highly oligomeric nature of the Fas DD–FADD DD complex in the intracellular region and its match in stoichiometry with the Fas-FasL interaction in the extracellular region ensures a highly cooperative and regulated mechanism to control this irreversible cell fate decision.

General DD assembly mechanisms

The current Fas DD–FADD DD complex structure and its similarity to that of the PIDD DD–RAIDD DD complex[17] provide another example of conserved interactions in the DD superfamily, which also include the caspase recruitment domain (CARD), the death effector domain (DED) and the Pyrin domain (PYD)[1]. The three types of interactions in the Fas DD–FADD DD and the PIDD DD–RAIDD DD complexes have been observed in the 1:1 Pelle DD–Tube DD complex[28], the 1:1 Apaf-1 CARD–caspase-9 CARD complex[29] and the 6:4:4 MyD88–IRAK4–IRAK2 complex[30] but not in the previously published Fas DD–FADD DD complex[16]. These interactions form the basis of a polymerization mechanism, which possesses intrinsic helical symmetry[30], in DD assembly. The different stoichiometries in these complexes despite the conservation of interactions establish DD superfamily members as versatile interactors and oligomerizers in signal transduction.

Accession codes. Protein Data Bank: Coordinates and structure factors for the core mFas–hFADD DD complex have been deposited under accession code 3OQ9. Protein Model Data Base: Coordinates for the 6 hFas–5 hFADD DD complex have been deposited under accession code PM0076550.

METHODS

Methods and any associated references are available in the online version of the paper at http://www.nature.com/nsmb/.

Note: Supplementary information is available on the Nature Structural & Molecular Biology website.

AUTHOR CONTRIBUTIONS
H.W. initiated the project and participated in project design and analysis; L.W. provided the samples for EM; L.W. and E.D. performed *in vitro* mutagenesis experiments; L.W. and Q.Y. performed multi-angle light scattering experiments; J.K.Y., L.W. and S.B.J. grew the crystals and collected the diffraction data; V.K. and H.W. solved the structure; E.D. performed the CD experiments and the salt-dependence experiments; A.J.R., S.R. and T.W. performed the EM experiments; A.C.C. and R.M.S. performed the cell biology experiments; A.Y.P. and C.V.R. performed the mass spectrometry experiments; H.W. made the figures and wrote the manuscript.

1. Park, H.H. *et al.* The death domain superfamily in intracellular signaling of apoptosis and inflammation. *Annu. Rev. Immunol.* **25**, 561–586 (2007).
2. Kohl, A. & Grutter, M.G. Fire and death: the pyrin domain joins the death-domain superfamily. *C. R. Biol.* **327**, 1077–1086 (2004).
3. Chinnaiyan, A.M., O'Rourke, K., Tewari, M. & Dixit, V.M. FADD, a novel death domain-containing protein, interacts with the death domain of Fas and initiates apoptosis. *Cell* **81**, 505–512 (1995).
4. Strasser, A., Jost, P.J. & Nagata, S. The many roles of FAS receptor signaling in the immune system. *Immunity* **30**, 180–192 (2009).
5. Wajant, H. The Fas signaling pathway: more than a paradigm. *Science* **296**, 1635–1636 (2002).
6. Kischkel, F.C. *et al.* Cytotoxicity-dependent APO-1 (Fas/CD95)-associated proteins form a death-inducing signaling complex (DISC) with the receptor. *EMBO J.* **14**, 5579–5588 (1995).
7. Huang, B., Eberstadt, M., Olejniczak, E.T., Meadows, R.P. & Fesik, S.W. NMR structure and mutagenesis of the Fas (APO-1/CD95) death domain. *Nature* **384**, 638–641 (1996).
8. Berglund, H. *et al.* The three-dimensional solution structure and dynamic properties of the human FADD death domain. *J. Mol. Biol.* **302**, 171–188 (2000).
9. Jeong, E.J. *et al.* The solution structure of FADD death domain. Structural basis of death domain interactions of Fas and FADD. *J. Biol. Chem.* **274**, 16337–16342 (1999).
10. Hill, J.M. *et al.* Identification of an expanded binding surface on the FADD death domain responsible for interaction with CD95/Fas. *J. Biol. Chem.* **279**, 1474–1481 (2004).
11. Martin, D.A. *et al.* Defective CD95/APO–1/Fas signal complex formation in the human autoimmune lymphoproliferative syndrome, type Ia. *Proc. Natl. Acad. Sci. USA* **96**, 4552–4557 (1999).
12. Rieux-Laucat, F., Le Deist, F. & Fischer, A. Autoimmune lymphoproliferative syndromes: genetic defects of apoptosis pathways. *Cell Death Differ.* **10**, 124–133 (2003).
13. Bettinardi, A. *et al.* Missense mutations in the Fas gene resulting in autoimmune lymphoproliferative syndrome: a molecular and immunological analysis. *Blood* **89**, 902–909 (1997).
14. Fisher, G.H. *et al.* Dominant interfering Fas gene mutations impair apoptosis in a human autoimmune lymphoproliferative syndrome. *Cell* **81**, 935–946 (1995).
15. Oliveira, J.B. & Gupta, S. Disorders of apoptosis: mechanisms for autoimmunity in primary immunodeficiency diseases. *J. Clin. Immunol.* **28** (Suppl 1), S20–S28 (2008).
16. Scott, F.L. *et al.* The Fas–FADD death domain complex structure unravels signalling by receptor clustering. *Nature* **457**, 1019–1022 (2009).
17. Park, H.H. *et al.* Death domain assembly mechanism revealed by crystal structure of the oligomeric PIDDosome core complex. *Cell* **128**, 533–546 (2007).
18. Siegel, R.M. *et al.* Measurement of molecular interactions in living cells by fluorescence resonance energy transfer between variants of the green fluorescent protein. *Sci. STKE* **2000**, PI1 (2000).
19. Vaishnaw, A.K. *et al.* The molecular basis for apoptotic defects in patients with CD95 (Fas/Apo-1) mutations. *J. Clin. Invest.* **103**, 355–363 (1999).
20. Carrington, P.E. *et al.* The structure of FADD and its mode of interaction with procaspase-8. *Mol. Cell* **22**, 599–610 (2006).
21. O' Reilly, L.A. *et al.* Membrane-bound Fas ligand only is essential for Fas-induced apoptosis. *Nature* **461**, 659–663 (2009).
22. Dhein, J. *et al.* Induction of apoptosis by monoclonal antibody anti-APO-1 class switch variants is dependent on cross-linking of APO-1 cell surface antigens. *J. Immunol.* **149**, 3166–3173 (1992).
23. Muppidi, J.R. & Siegel, R.M. Ligand-independent redistribution of Fas (CD95) into lipid rafts mediates clonotypic T cell death. *Nat. Immunol.* **5**, 182–189 (2004).
24. Holler, N. *et al.* Two adjacent trimeric Fas ligands are required for Fas signaling and formation of a death-inducing signaling complex. *Mol. Cell. Biol.* **23**, 1428–1440 (2003).
25. Tibbetts, M.D., Zheng, L. & Lenardo, M.J. The death effector domain protein family: regulators of cellular homeostasis. *Nat. Immunol.* **4**, 404–409 (2003).
26. Yang, J.K. *et al.* Crystal structure of MC159 reveals molecular mechanism of DISC assembly and FLIP inhibition. *Mol. Cell* **20**, 939–949 (2005).
27. Siegel, R.M. *et al.* SPOTS: signaling protein oligomeric transduction structures are early mediators of death receptor-induced apoptosis at the plasma membrane. *J. Cell Biol.* **167**, 735–744 (2004).
28. Xiao, T., Towb, P., Wasserman, S.A. & Sprang, S.R. Three-dimensional structure of a complex between the death domains of Pelle and Tube. *Cell* **99**, 545–555 (1999).
29. Qin, H. *et al.* Structural basis of procaspase-9 recruitment by the apoptotic protease-activating factor 1. *Nature* **399**, 549–557 (1999).
30. Lin, S.C., Lo, Y.C. & Wu, H. Helical assembly in the MyD88–IRAK4–IRAK2 complex in TLR/IL-1R signalling. *Nature* **465**, 885–890 (2010).

ONLINE METHODS

Cloning, protein expression and purification. Initial hFas DD (residues 205–335, no tag) and hFADD DD (residues 93–208, His tagged) constructs were copurified to form the hFas–hFADD complex, which was trimmed by limited proteolysis to derive the constructs used for subsequent polycistronic coexpressions in pET28a: hFas DD (residues 218–318) with hFADD DD (residues 93–191, C-terminally His tagged), and mFas DD (residues 210–310) with hFADD DD (residues 93–184, C-terminally His tagged). The coexpression constructs were transformed into *Escherichia coli* BL21(DE3) RIPL cells. Transformed cells were grown at 37 °C in LB medium containing 35 µg ml^{-1} kanamycin and induced at 20 °C with 0.4 mM IPTG for an additional 20 h. The Fas–FADD complexes were purified by nickel-affinity ion exchange chromatography using UnoQ (Bio-Rad) and by gel filtration using Superdex 200 (GE Healthcare).

Electron microscopy and image processing. Samples were negatively stained with uranyl formate[31]. Images were collected on imaging plates with a Tecnai T12 electron microscope (FEI) equipped with an LaB$_6$ filament and operated at 120 kV. Imaging plates were read out with a Ditabis micron imaging plate scanner (DITABIS)[32], and 2 × 2 pixels were averaged to yield a pixel size of 4.5 Å on the specimen level. Particles were selected using WEB, and the SPIDER software package[33] was used for further image processing. 10,397 particles of hFas DD–hFADD DD complex were selected from 135 micrographs, and 15,271 mFas DD–hFADD DD complex particles from 121 micrographs. Particles were windowed into 48 × 48 pixel images and subjected to ten cycles of multi-reference alignment. Each round of multi-reference alignment was followed by K-means classification specifying 100 output classes. For comparison with the previously published tetrameric Fas DD–FADD DD structure (PDB ID code 3EZQ)[16] and with the current structure of the 5:5 complex, the atomic models were filtered to a 25-Å resolution, and projections were calculated at an angular interval of 30°. The projections from the two sets matching best with class averages were identified using the cross-correlation function in SPIDER.

Mass spectrometry. The mFas–hFADD and hFas–hFADD DD complexes were buffer exchanged into 500 mM ammonium acetate at pH 8.0 using Bio-Spin columns (Bio-Rad). Nanoflow electrospray ionization (nESI-MS) and tandem MS experiments were conducted on a high-mass Q-ToF2 mass spectrometer (Waters)[34]. Typically, 2 µl of the aqueous protein samples were electrosprayed from a gold-coated borosilicate capillary prepared in house[35]. The following instrument parameters were used: capillary voltage, 1.8 kV; cone voltage, 100 V; extractor cone, 5 V, and microchannel plate 2, 2,400 V, with a backing pressure of ~0.5 bar. For the tandem MS experiments, the relevant m/z value was selected for the quadrupole, and a collision energy of 50–100 V was applied at an argon pressure of 3.0×10^{-2} mbar. Cesium iodide was used for calibration.

Multi-angle light scattering (MALS) analysis. Protein samples were injected into a Superdex 200 (10/300 GL) gel filtration column (GE Healthcare), equilibrated with a buffer containing 20 mM Tris, pH 8.0, and 100 mM NaCl. The chromatography system was coupled to a three-angle light scattering detector (mini-DAWN TRISTAR) and a refractive index detector (Optilab DSP) (Wyatt Technology). Data analysis was carried out using ASTRA V.

Crystallization and structure determination. The mFas DD–hFADD DD complex was crystallized in 0.1 M Tris pH 8.5, 100 mM MgCl$_2$, 5% glycerol and 6–10% PEG4000. Diffraction data were collected at 100 K at the NE-CAT beam line of APS and processed with HKL2000[36]. The hFas and hFADD layers were generated based on the PIDD–RAIDD complex structure[17] using PDB codes 1DDF[7] and 3EZQ[16], respectively, and used for molecular replacement with Phaser[37]. Additional molecular replacement searches using the Fas monomer after fixing the 5:5 complex did not find more molecules in the crystal. Consistently, the sixth and seventh Fas molecules in the same locations as the two additional RAIDD molecules in the PIDD–RAIDD complex would have caused steric clashes in the crystal. Therefore, the mFas–hFADD crystal contains only the core 5:5 complex. Rigid-body refinement in CNS[38] gave an R of 44.6% and an R_{free} of 44.7%. The hFas in the complex was then used to model the mFas structure, and the

mFas–hFADD complex was subjected to one round of minimization with strict non-crystallographic symmetry, which brought down the R and R_{free} to 35.4% and 34.9%, respectively (**Table 1**). Further validation of the structure using alternative arrangements is shown in **Supplementary Table 2**. The final atomic model shows r.m.s. deviations of 0.26Å and 0.20Å from the NMR structure of hFas DD (1DDF) and the crystal structure of hFADD DD (1EZQ), respectively. All superpositions were performed with lsqman in CCP4[39]. Structural presentations were generated using Pymol (DeLano Scientific)[40], and surface electrostatic calculations were performed according to Baker *et al.*[41].

His-tag pull-down assay. Coexpressed wild-type and mutant Fas DD and His-tagged FADD DD proteins were purified with Ni-NTA resin, except that the incubation with Ni-NTA resin was done at 37 °C to mimic the *in vivo* condition. The eluates were subjected to 18% SDS-PAGE with the tricine buffer system.

Fluorescence resonance energy transfer (FRET) assay. Full-length human wild-type or mutant Fas or Fas lacking the death domain (Fas ΔDD) was cloned into pEYFP-N1 (Clontech). Human wild-type or mutant FADD DD was cloned into pECFP-C1 (Clontech). After confirming protein expression, 2 µg of each construct in varied combinations was transfected into 293T cells using Fugene 6 (Roche). Cells were analyzed 48 h after transfection by flow cytometric detection of FRET as previously described[18,42], using a CyAn ADP flow cytometer (Dako) with 405-nm/488-nm dual laser excitation. FRET data are shown for cells gated for similar expression of the CFP and YFP fusion proteins. Change in geometric mean fluorescence intensity (ΔMFI) was calculated by subtracting the MFI of non-interacting proteins (Fas ΔDD with WT FADD DD) from the MFI in the FRET channel of interacting pairs. They are displayed in biexponential plots to allow accurate analysis of the FRET signal[43].

Apoptosis assay of Fas mutants. Wild-type or mutant hFas cDNA was electroporated into Jurkat E6.1 cells as previously described[11]. For induction of cell death, 2×10^5 viable cells (1×10^6 cells per ml) were incubated in the absence or presence of increasing amounts of anti-Fas Apo 1-3 (Alexis) cross-linked 1:10 with anti-mouse IgG3 (eBioscience), or increasing amounts of recombinant FasL oligomerized through a leucine-zipper tail[42] for 6–8 h. Specific cell death was quantified via flow cytometry using annexin V as previously described[11].

31. Ohi, M., Li, Y., Cheng, Y. & Walz, T. Negative staining and image classification—powerful tools in modern electron microscopy. *Biol. Proced. Online* **6**, 23–34 (2004).
32. Li, Z., Hite, R.K., Cheng, Y. & Walz, T. Evaluation of imaging plates as recording medium for images of negatively stained single particles and electron diffraction patterns of two-dimensional crystals. *J. Electron Microsc. (Tokyo)* **59**, 53–63 (2010).
33. Frank, J. *et al.* SPIDER and WEB: processing and visualization of images in 3D electron microscopy and related fields. *J. Struct. Biol.* **116**, 190–199 (1996).
34. Sobott, F., Hernandez, H., McCammon, M.G., Tito, M.A. & Robinson, C.V. A tandem mass spectrometer for improved transmission and analysis of large macromolecular assemblies. *Anal. Chem.* **74**, 1402–1407 (2002).
35. Hernández, H. & Robinson, C.V. Determining the stoichiometry and interactions of macromolecular assemblies from mass spectrometry. *Nat. Protoc.* **2**, 715–726 (2007).
36. Otwinowski, Z. & Minor, W. Processing of X-ray diffraction data collected in oscillation mode. *Methods Enzymol.* **276**, 307–326 (1997).
37. Read, R.J. Pushing the boundaries of molecular replacement with maximum likelihood. *Acta Crystallogr. D Biol. Crystallogr.* **57**, 1373–1382 (2001).
38. Brunger, A.T. *et al.* Crystallography & NMR system: a new software suite for macromolecular structure determination. *Acta Crystallogr. Biol. Crystallogr.* **54**, 905–921 (1998).
39. Collaborative Computational Project. N. The CCP4 suite: programs for protein crystallography.. *Acta Crystallogr. D Biol. Crystallogr.* **50**, 760–763 (1994).
40. Delano, W.L. *The PyMol Molecular Graphics System* (Delano Scientific, 2002).
41. Baker, N.A., Sept, D., Joseph, S., Holst, M.J. & McCammon, J.A. Electrostatics of nanosystems: application to microtubules and the ribosome. *Proc. Natl. Acad. Sci. USA* **98**, 10037–10041 (2001).
42. Siegel, R.M. *et al.* Fas preassociation required for apoptosis signaling and dominant inhibition by pathogenic mutations. *Science* **288**, 2354–2357 (2000).
43. Herzenberg, L.A., Tung, J., Moore, W.A. & Parks, D.R. Interpreting flow cytometry data: a guide for the perplexed. *Nat. Immunol.* **7**, 681–685 (2006).

Supplementary information

The Fas–FADD death domain complex structure reveals the basis of DISC assembly and disease mutations

Liwei Wang, Jin Kuk Yang, Venkataraman Kabaleeswaran, Amanda J. Rice, Anthony C. Cruz, Ah Young Park, Qian Yin, Ermelinda Damko, Se Bok Jang, Stefan Raunser, Carol V. Robinson, Richard M. Siegel, Thomas Walz & Hao Wu

Supplementary Table 1. MALS measurements of the mFas–hFADD and the hFas–hFADD complexes

mFas–hFADD complex: 119.6 kDa in average
Calculated mass
   5 mFas–5 hFADD = 117.6 kDa
   6 mFas–5 hFADD = 129.4 kDa
   7 mFas–5 hFADD = 141.1 kDa

Peak concentration based on RI	Peak light scattering signal	Molecular mass (error)
0.28 mg/ml	1.9	122.5 kDa (1%)
0.35 mg/ml	2.5	128.4 kDa (0.5%)
0.38 mg/ml	2.5	116.5 kDa (1%)
0.58 mg/ml	3.8	119.4 kDa (0.9%)
0.80 mg/ml	5.5	111.1 kDa (1%)

hFas–hFADD complex: 115.7 kDa in average
Calculated mass
   5 hFas–5 hFADD = 119.8 kDa
   6 hFas–5 hFADD = 131.2 kDa
   7 hFas–5 hFADD = 142.6 kDa

Peak concentration based on RI	Peak light scattering signal	Molecular mass (error)
0.18 mg/ml	1.1	107.3 kDa (3%)
0.19 mg/ml	1.1	108.5 kDa (1%)
0.51 mg/ml	3.0	111.9 kDa (0.9)
0.65 mg/ml	5.3	136.0 kDa (0.7%)
0.91 mg/ml	5.5	115.1 kDa (2%)
0.95 mg/ml*	6.1	115.2 kDa (0.3%)
0.55 mg/ml*	3.2	115.5 kDa (2%)
0.26 mg/ml*	1.4	115.1 kDa (3%)

*These three samples were from the same protein preparation

Supplementary Table 2. The molecular replacement solution and other alternative structures

Resolution	Model	R	Rfree
20-6.8Å	5 mFas: 5 hFADD	0.354	0.349
20-6.8Å	Exchanged layers 5 hFADD: 5 mFas	0.411	0.426
20-6.8Å	4 mFas: 5 hFADD	0.383	0.361
20-6.8Å	5 mFas: 4 hFADD	0.376	0.395
20-6.8Å	4 mFas: 4 hFADD	0.402	0.414
20-6.8Å	5 RAIDD-Ala: 5 PIDD-Ala	0.437	0.444
20-6.8Å	Exchanged layers 5 PIDD-ALA: 5RAIDD-ALA	0.463	0.509

Supplementary Table 3. Single site Fas DD mutations in ALPS

ALPS Mutations		Accessibility	Interface type	Interaction with FADD	Number of occurrences
In precursor	In mature chain	Alone			
Y232C	Y216C	Exposed		+	0
T241P	T225P	Exposed			
V249L	V233L	Buried			
R250Q	R234Q	Exposed	Ib	-	2
R250P	R234P				
G253S	G237S	Exposed			
G253D	G237D				
A257D	A241D	Exposed	IIIa	-	5
I259R	I243R	Buried			
D260Y	D244Y	Exposed	IIIa	-	5
D260V	D244V				
D260G	D244G				
I262N	I246N	Buried			
Q268P	Q252P	Exposed			
T270K	T254K	Exposed	IIIb	-	3
T270I	T254I				
E272K	E256K	Exposed	Ia	-	5
E272G	E256G				
L277R	L261R	Buried			
I310S	I294S	Buried			

The mutation list was obtained from
http://research.nhgri.nih.gov/ALPS/fas_tnfrsf6_exon9_mut.shtml.
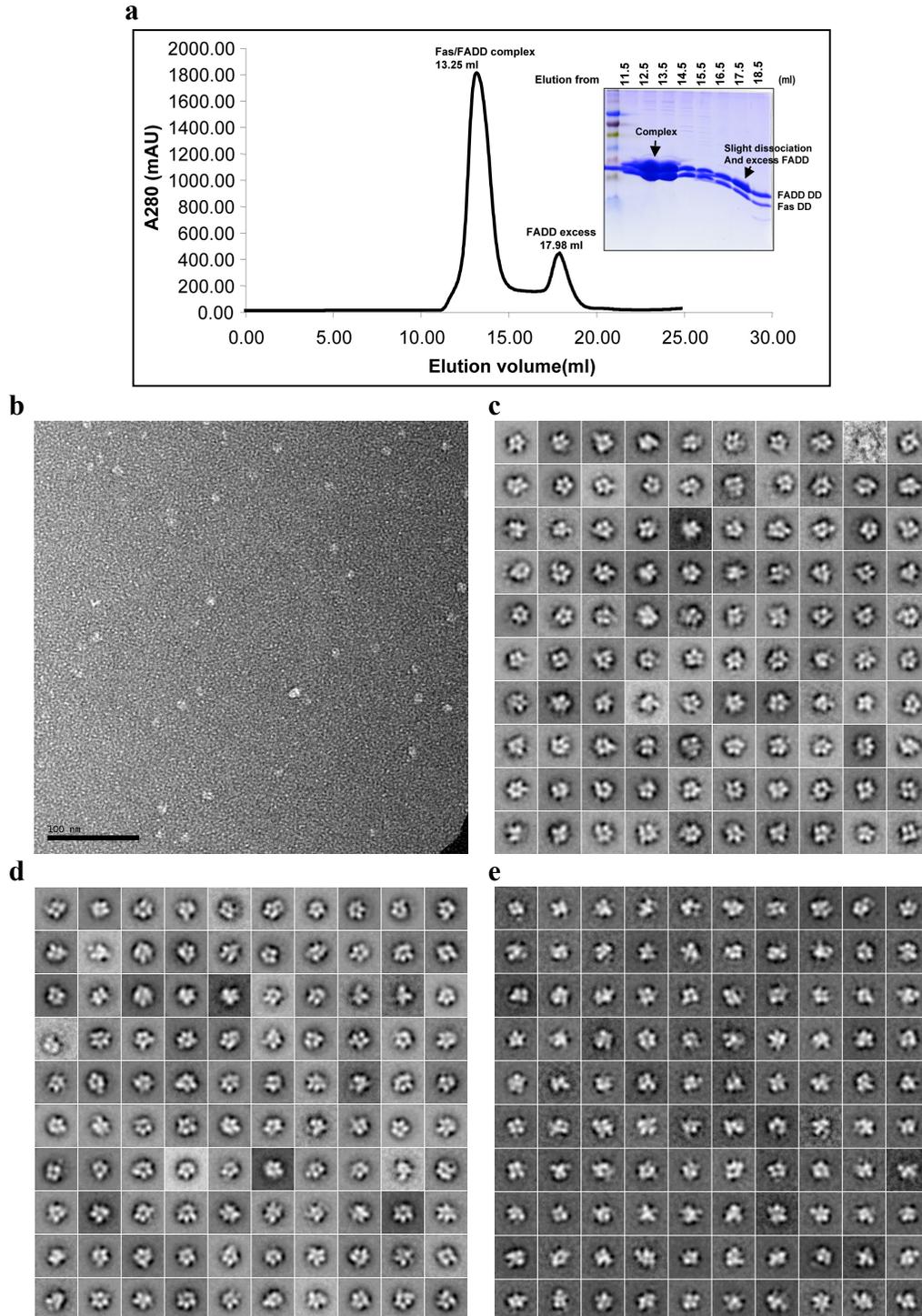Mutations that were tested in this report are denoted in red.

Supplementary Table 4. Previously published FADD DD mutations

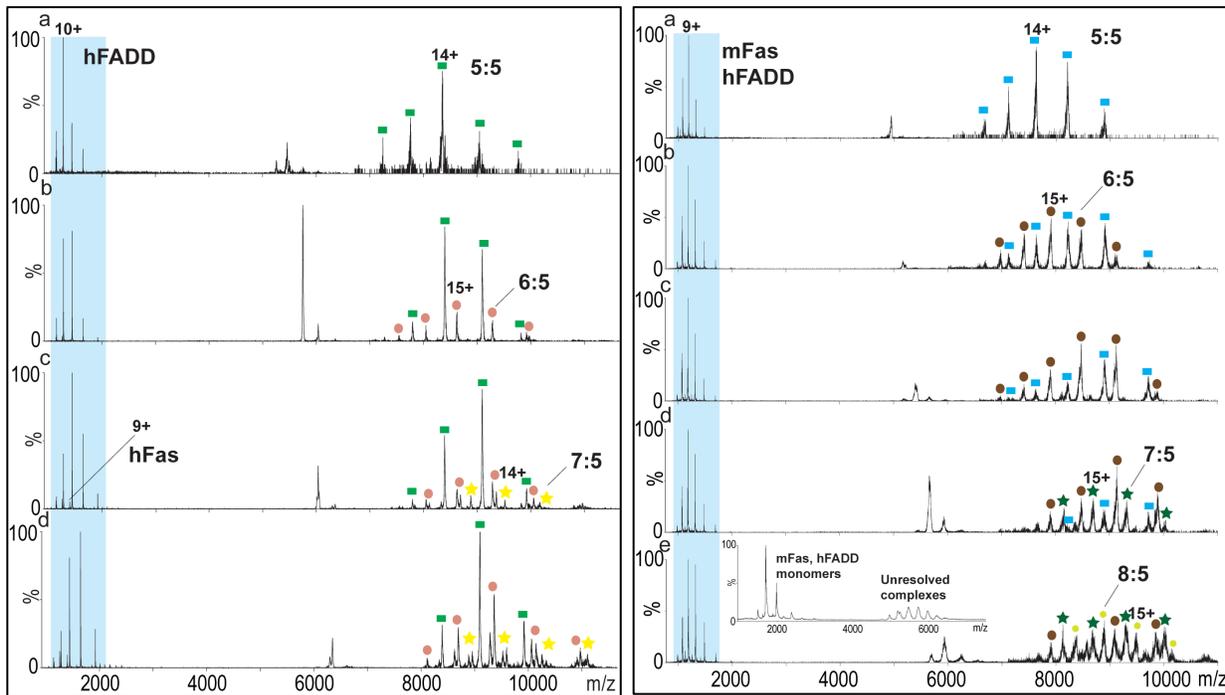| FADD Mutations	Side chain		Interface Type	Interaction	Number of occurrences	Reference
	Alone	Complex				
E95R	Exposed	Exposed	Other	+		1
A99E	Exposed	Exposed	Other	+		1
D106A	Exposed	Exposed	Other	-		1
Mouse R110A	Exposed	Exposed	IIIb	-	5	2
Mouse D111A	Exposed	Buried	Other	+		2
Mouse K113A	Buried	Buried	Other	-		2
R113E	Buried	Buried	Other	-		1
Mouse R114A	Exposed	Exposed	Ib	+/-	5	2
R117E	Exposed	Buried	Ib	-	5	1
Mouse R117A	Exposed	Buried	Ib	-	5	2
Mouse E118A	Exposed	Exposed	Ib	-	5	2
Mouse L119N	Buried	Buried	Other	+/-		2
Mouse K120A	Exposed	Exposed	Ib	+	5	2
Mouse V121N	Buried	Buried	Other	-		2
Mouse E123A	Exposed	Buried	IIIa	-	3	2
D123R	Exposed	Buried	IIIa	-	3	1
K125A	Exposed	Exposed	Other	-		1
Mouse D127A	Exposed	Exposed	IIIa	+/-	3	2
Mouse E130A	Exposed	Exposed	Ib	+	5	2
Mouse E131A	Exposed	Exposed	IIIa	+	3	2
E139R	Exposed	Exposed	Ia	+	2	1
R142A	Exposed	Buried	Ia	-	2	1
R142E	Exposed	Buried	Ia	-	2	1
R146A	Exposed	Exposed	Ia	-	2	1
E152A	Exposed	Exposed	Other	+		1
R166E	Exposed	Exposed	IIb	-	5	1
Q169A	Exposed	Exposed	IIb	+/-	5	1
L172E	Exposed	Exposed	IIb	-	5	1
D175R	Exposed	Exposed	IIb	-	5	1

All residues are for the human sequences except where noted.

1. Hill, J.M. et al. Identification of an expanded binding surface on the FADD death domain responsible for interaction with CD95/Fas. J Biol Chem 279, 1474-81 (2004).
2. Jeong, E.J. et al. The solution structure of FADD death domain. Structural basis of death domain interactions of Fas and FADD. J Biol Chem 274, 16337-42 (1999).
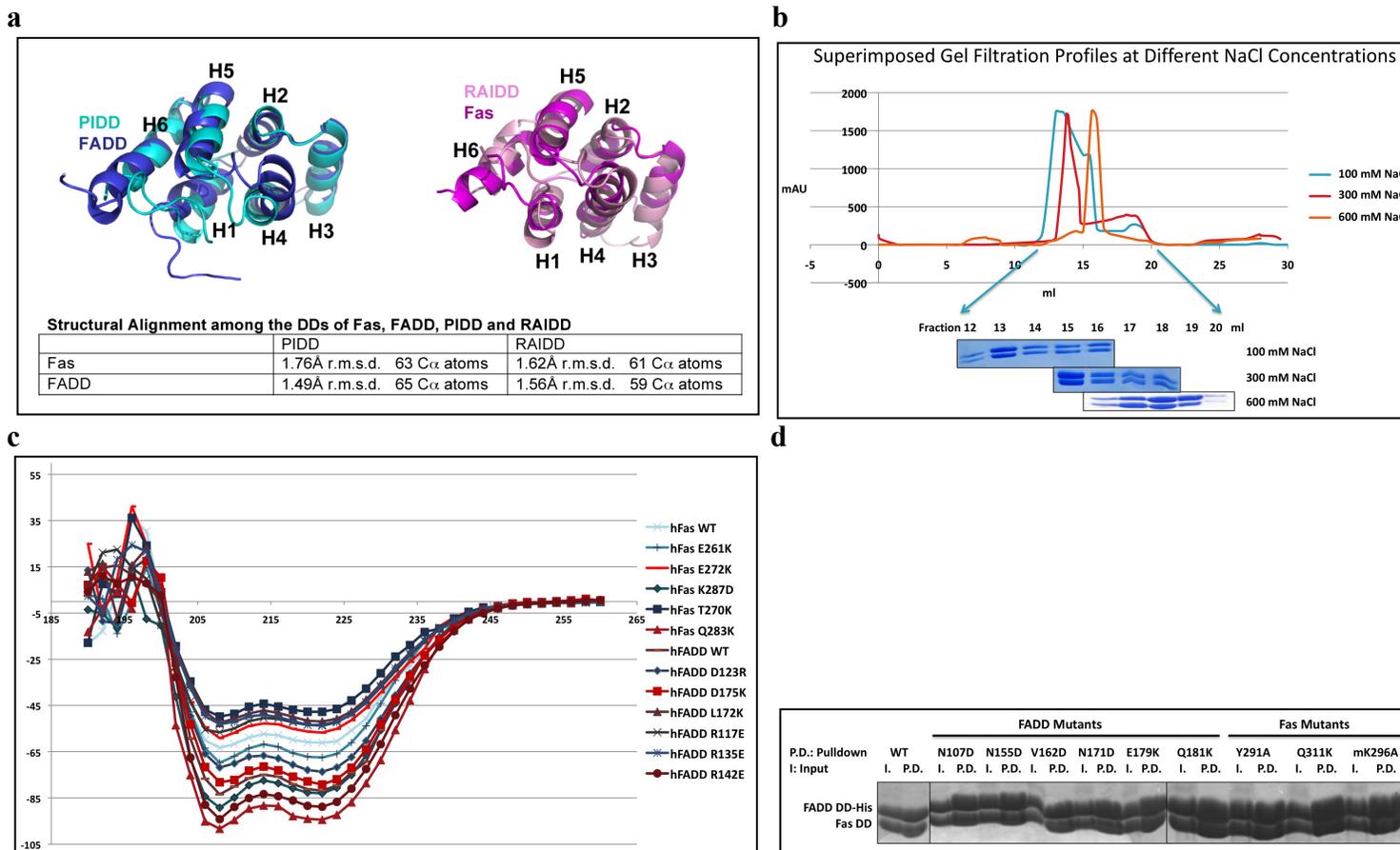
Supplementary Figure 1. Electron microscopy analyses of the Fas–FADD and the PIDD–RAIDD complexes. (a) Gel filtration profile of the human Fas DD–human FADD DD complex and SDS-PAGE of the fractions. (b) Electron micrograph of the hFas DD–hFADD DD complex negatively stained with uranyl formate. The scale bar is 100 nm. (c) Class averages obtained by classifying 10,397 particle images of the hFas DD–hFADD DD complex into 100 classes. Side length of the individual panels is 23 nm. (d) Class averages obtained by classifying 15,271 particle images of the mFas DD–hFADD DD complex into 100 classes. (e) Class averages obtained by classifying 11,105 particle images of the PIDD DD–RAIDD DD complex into 100 classes. Note the similarity to the class averages obtained for the Fas DD–FADD DD complex.

Supplementary Figure 2. Tandem mass spectra of the Fas–FADD complexes. Left: the hFas–hFADD complex. The peaks centered at a. 5024, b. 5242, c. 5481, and d. 5742 m/z were isolated and collision energy (50-100V) was applied. At lower m/z monomers of hFas (centered at 9^+ ion) and hFADD (centered at 10^+ ion) dissociate from the complex and leave 'stripped' complexes at high m/z. In all spectra the stripped complex for the 5:5 complex was observed. The stripped complexes losing either hFas or hFADD for the 6:5 and 7:5 complex were detected in b, c, d and c, d, respectively. Right: the mFas–hFADD complex. The peaks centered at a. 4947, b. 5168, c. 5401, d. 5669, and e. 5913 m/z were isolated and collision energy (50-100V) was applied. Monomers of mFas and hFADD, centered at 9^+ ion at lower m/z, dissociate from the complex and leave 'stripped' complexes at high m/z. In all spectra the stripped complex for the 5:5 complex was observed. The 6:5 and 7:5 complexes were detected in b, c, d, e and d, e, respectively. Minor species of the 8:5 complex were detected in e. Inset in e, mass spectrum of mFas–hFADD at the concentration of 3 µM. Monomers of mFas and hFADD at lower m/z and higher oligomeric species were observed at high m/z.

Supplementary Figure 3. Structural, biochemical and mutational analyses of the Fas–FADD interaction. (a) Fas DD is more similar to RAIDD DD and FADD DD is more similar to PIDD DD. (b) Salt dependence of the hFas–hFADD complex formation. The complex started to dissociate at ~300 mM NaCl. (c) Superimposed CD spetra of WT and mutant Fas and FADD DDs. (d) Mutations of conserved Fas and FADD surface residues that do not map to the observed structural interface. These mutations have no effects in the mutual interaction between Fas and FADD. All mutations were performed on the human sequences except that the human Fas K296 residue was tested with the equivalent K296A mutation in the mouse sequence because we already have this mutation as a surface entropy mutation for improving crystallization.

Supplementary Figure 4. The previously published Fas–FADD complex structure. (a, b, c) Mapping of residues whose mutations are associated with ALPS and cause defective FADD DD interaction onto the surface of the previously published Fas DD–FADD DD complex structure (PDB ID code 3EZQ), showing that the residues are not at the interaction interface. Fas DDs are shown in grey (top front), blue (bottom front), light blue (left back) and black (right back), respectively. FADD DDs are shown in cyan. Locations of R250 (red), A257 (magenta), D260 (orange), T270 (yellow) and E272 (green) are shown. Similarly, structurally identified disruptive mutations of Fas are not located at the interface, but the exposed surface, of the previously published Fas DD-FADD DD complex structure. (a) The tetrameric structure. (b) and (c) Two sides of a Fas–FADD interaction pair, showing the locations of disruptive mutations. (d) Calculated projections from the previously published crystal structure of the Fas DD–FADD DD complex (PDB ID code 3EZQ). The structure (top row) was low-pass filtered (cutoff, 25 Å) (middle row) and projections (bottom row) were calculated at an angular interval of 30°. The Euler angles (φ, θ, ψ), which define the orientation of the complex, are given above each column. Note the dissimilarity to the EM class averages. Scale bars are 10 nm. (e) Structural alignment of NMR structure of hFas DD (magenta, PDB code 1DDF) with the hFas structure in the published hFas DD–hFADD DD complex structure (gray, PDB code 1EZQ). Helices 5 and 6 of hFas DD in the published complex have merged into one long helix, with an additional helix at the C-terminus.